Available online at www.sciencedirect.com
ScienceDirect
Journal of Power Sources 161 (2006) 437–443
JOURNAL OF POWER SOURCES
www.elsevier.com/locate/jpowsour

Characterization of electrolyte–electrode interlayers in thin film solid oxide fuel cells

Thomas L. Reitz [a,*], Haiming Xiao [b]

[a] *Propulsion Directorate, Air Force Research Laboratory Wright-Patterson AFB, OH 45433-7251, United States*
[b] *Aerospace Power and Propulsion, UES Corp. Dayton, OH 45432-1894, United States*

Received 2 March 2006; received in revised form 14 April 2006; accepted 19 April 2006
Available online 30 May 2006

Abstract

In order to reduce the operating temperature of solid oxide fuel cells (SOFCs), anode-supported cells incorporating thin film (∼10 μm) electrolytes in conjunction with anode/electrolyte and cathode/electrolyte interlayers were studied. SOFC button cells were prepared through deposition of colloidal slurries onto anode supported substrates and were analyzed as a function of temperature and polarization via voltammetry and electrochemical impedance spectroscopy (EIS). It was found that the electro-catalytic activity or electrode/electrolyte interfacial areas were enhanced through the addition of these interlayers. This performance improvement was attributed to the introduction of a diffuse mixed conduction region associated with these interlayers. The cathode is thought to benefit disproportionately from this enhancement. Single SOFC button cells with electrode interlayers were then characterized as a function of temperature and polarization to assess the involvement of these interfacial layers. EIS was applied and the data were used to deconvolute component impedances. Finally electrochemical models were developed to provide a more complete understanding of these assemblies under operation.

Keywords: Solid oxide fuel cells; EIS; Thin films; Zirconia

1. Introduction

Solid oxide fuel cells (SOFCs) are energy conversion devices that produce electricity by electrochemically combining reactions of fuel and oxidant gases across an ionic-conducting ceramic. SOFCs are anticipated to become very competitive devices for electrical power generation because of their high efficiency and lower pollution potential. SOFCs are an attractive option relative to polymer electrolyte fuel cells because they exhibit greater fuel tolerance, higher efficiencies, and produce high-grade waste heat making them suitable for combined heat and power applications. SOFCs are reaching pre-commercialization with several hundreds of residential stationary power units (∼1 kW) being tested and larger units (250 kW or above) being evaluated by various utility companies world wide [1,2]. Although great progress has been made, at present the SOFC technology is still in its developmental (or pre-commercialization) stage and several technical challenges remain to be solved before it becomes a practical power system.

In conventional SOFCs, the electrolyte is yttria-stabilized zirconia (YSZ) with thickness of ∼200 μm necessitating an operating temperature of around 900–1000 °C. These high operating temperatures place considerable constraints on materials used for interconnections, current collectors, manifolds, and seals. Because these exotic materials are often cost prohibitive, lowering the operation temperature below 750 °C is critical for ensuring SOFC's cost effectiveness. In order to achieve these temperature decreases, many researchers have explored the use of thin film electrolytes with high degrees of success [3–5]. While these thin film electrolytes do enable operation at lower temperature, activation polarization, especially on the cathode are significantly more pronounced under these conditions. This is primarily attributed to the sluggish kinetics associated with decreased temperature operation [6]. Others have explored the application of thin film composite interlayers as a means to improve charge transfer reaction in the electrode/electrolyte interface for both anode and cathode [7–10]. The nature of these interlayers is still a matter of contention and further studies are

* Corresponding author. Tel.: +1 937 255 4275; fax: +1 937 656 7529.
E-mail address: Thomas.reitz@wpafb.af.mil (T.L. Reitz).

0378-7753/$ – see front matter © 2006 Published by Elsevier B.V.
doi:10.1016/j.jpowsour.2006.04.019

required to adequately understand their function. The objective of this effort was to characterize the anode and cathode performance enhancement of thin film, anode-supported SOFCs when anode and cathode interlayers are included between the electrode and electrolyte interface. SOFC button cells containing the interlayers were evaluated as a function of temperature and polarization. EIS was used to generate a more complete understanding of how these interfaces improve cell performance. Finally, models were prepared based upon polarization and impedance data which provide valuable insight into the relative magnitudes of the impedance contributions.

2. Experimental

Test cells were generally constructed through a five-layer process which includes: (a) porous Ni + YSZ anode support; (b) anode/electrolyte interlayer; (c) dense YSZ electrolyte; (d) cathode/electrolyte interlayer; (e) porous LSM ($(La_{0.85}\ Sr_{0.15})_{0.98}MnO_{3-x}$) cathode ($x = 0.103$). This study's focus was to evaluate the impact of a thin film layer which acts to transition the structural and conducting properties from electrolyte to electrode. Typical interlayer compositions employed in this study were 50%YSZ–50%LSM for cathode/electrolyte and 50%YSZ–50%NiO for anode/electrolyte.

The cell fabrication process is briefed as follows: NiO and YSZ materials were purchased from Alfa Aesar and Tosoh respectively and were mixed in requisite proportions (70% NiO–30% YSZ) then ball milled with measured amounts of rice flour or carbon to induce porosity. The ball-mill was conducted in a wet process with 5 mm diameter YSZ balls and ethanol-based solvent as media. The mixed powders were dried then unaxially die-pressed into discs of ~3.3 cm in diameter and ~1.2 mm of thickness. Colloidal slurries of anode/electrolyte interlayer and electrolyte with ethanol–toluene as solvents or dispersants were sequentially sprayed on the anode discs. The coated discs were sintered in air at 1400 °C for 2 h using a controlled ramp process. Cathode interlayer and LSM cathode slurries were pasted onto the half cells, respectively, to make complete button cells. The thickness of both anode and cathode interlayers was controlled at ~20 μm while that of the electrolyte was controlled at ~10 μm, which was demonstrated in scanning electron microscopy (SEM) images [10]. The cathode surface area was controlled to a known value so that current density can be calculated for electrochemical measurements.

Four probe electrochemical measurements were accomplished by attaching two platinum wires to each side of the button cell, i.e., anode and cathode. The anode supported button cell was sealed onto an alumina tube (Vesuvius) with high temperature cement (Cerambond 552, Aremco Products Inc.). A specially-designed quartz fixture for feeding fuel gas and releasing exhaust gas was connected to the alumina tube through a compression fitting (Swagelok). Sealing around the anode leads was accomplished through two threaded bushings with silicon rubber septums (ACE Glass) which were attached to the quartz fixture via a graded seal. The complete cell was then placed into the isothermal zone of a clam-shell furnace. Reduction of the NiO to Ni was achieved through a controlled temperature ramp in an anode flow stream of 10% H_2, balance N_2. Thermal Gravimetric Analysis (TGA) determined that 98% of NiO was reduced by 380 °C in pure hydrogen suggesting that complete reduction of the anode would be achieved by 450 °C. No significant difference in cell performance was observed as a function of reduction temperature in the range of 600–800 °C. After the anode reduction was complete, the cell was brought to the desired temperature for testing and the reactant gas was switched to humidified hydrogen gas. The cathode chamber is not sealed, so a purified air stream was blown over the surface to ensure ample oxygen availability. Electrochemical characterization was conducted using Solartron 1260 Impedance gain/phase analyzer coupled to a Solartron 1287 Electrochemical Interface. Complete cell assemblies were evaluated electrochemically to ensure that hermeticity was achieved. Open circuit voltages (OCVs) were nominally 1.05–1.12 V. A pictorial representation of the completed cell, the test fixture, and a more detailed description of cell continuity analysis are provided elsewhere [10].

3. Results and discussion

It has been previously observed that the application of a thin electrode interlayer between the bulk electrode structure and dense electrolyte membrane can significantly increase cell performance [4]. These electrode interlayers typically involve reducing the concentrations of active material (e.g. Ni or LSM) while increasing the concentration of support phase (YSZ) in order to induce greater homogeneity with the dense electrolyte membrane. A polarization curve illustrating the impact of these interlayers on a typical fuel cell is presented (Fig. 1). A maximum power density in excess of 0.9 W cm^{-2} was achieved for the specimen containing the thin, interfacial layers which was far better than the sample without electrode/electrolyte interlayers.

An OCV of 1.08 V was observed for the five-layer assembly which is slightly higher than that observed for the three-layer assembly, ~1.00 V. Improvement in the OCV of the cell was likely due to fact that the addition of interlayers (LSM–YSZ cathode interlayer and Ni-richer YSZ anode interlayer) balanced the thermal expansion between single LSM cathode, YSZ elec-

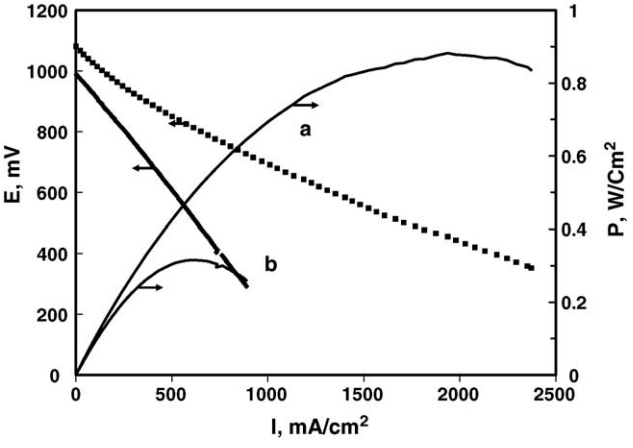

Fig. 1. Polarization curves for single SOFC button cells at 800 °C: (a) five-layer assembly and (b) three-layer assembly.

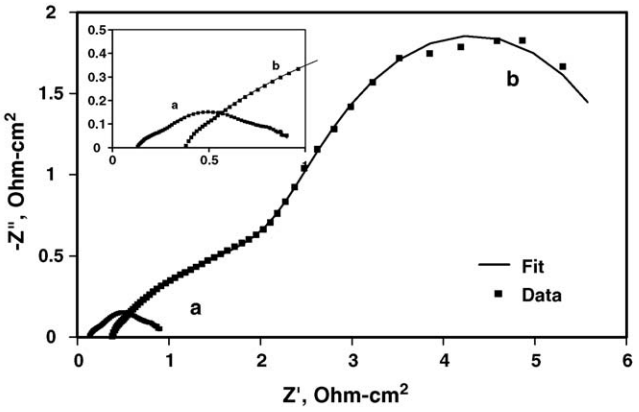

Fig. 2. Impedance spectra obtained for single SOFC button cells at 750 °C, (a) three-layer assembly, (b) three-layer assembly.

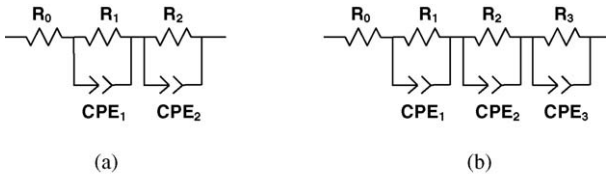

R_0: Ohmic resistance
R_1: High frequency semicircle resistance
CPE_1 High frequency semicircle constant phase element, $Z = 1/C(i\bullet\ \omega)^{\alpha}$
R_2: Mid-Range Frequency semicircle resistance
CPE_2: Mid-Range Frequency semicircle constant phase element
R_3: Low Frequency semicircle resistance
CPE_3: Low Frequency semicircle constant phase element

Fig. 3. Equivalent circuits of model fitting for impedance spectra obtained for single SOFC button cells: (a) three-layer assembly and (b) five-interlayer assembly.

trolyte film, and Ni–YSZ support anode which improved the integrity of YSZ electrolyte. The thermal expansion coefficient (TEC) of the YSZ electrolyte is $\sim 10 \times 10^{-6}$ cm(cm K)$^{-1}$, while LSM is $\sim 12 \times 10^{-6}$ cm(cm K)$^{-1}$ and Ni–YSZ cermet anode is $\sim 13 \times 10^{-6}$ cm(cm K)$^{-1}$.

One can see in Fig. 1 that overpotentials associated with the cell lacking interlayers (curve b) appear to be very significant but with no apparent non-linear features occurring at the low current densities. The nature of the electrode reaction kinetics was better examined by EIS, and will be discussed later in this section. Tafel slopes for the cell incorporating the interlayers (curve a) and the cell without (curve b) are similar at lower current densities.

More insight into these differences can be observed by examination of their respective impedance spectra (Fig. 2). Two clear time constants are observed for the three-layer assembly with the low frequency (<10 Hz) feature appearing significantly more capacitive than the high frequency arc. The low frequency feature was associated with the cathode through variation of gas compositions which is consistent with literature [11]. The five-layer specimen contains three distinct time constants with the predominant semicircular feature appearing between the frequencies of 10–10^3 Hz (Fig. 2a). As could be expected through examination of Fig. 1, the five-layer specimen exhibits far less total impedance than that observed for the three-layer. One obvious explanation for this observation is that the ionic conductivity of the LSM cathode is limited while the Ni/YSZ anode is high in both electronic and ionic conduction. Introduction of YSZ into the electrode/electrolyte interlayer will result in a substantial increase in the ionic conductivity of the cathode interlayer and improve cathode performance disproportionately relative to the anode wherein only a small change in the YSZ concentration has been made. Secondly, it has been well accepted that introduction of transition interlayers between the electrodes and the electrolytes increase the triple phase boundary region expanding the number of sites available for electrochemical activity.

Model fitting with equivalent circuit diagrams indicate that the cell without interlayer addition (Fig. 2b) is adequately fit to a circuit diagram as shown in Fig. 3-a. However, the specimen containing anode and cathode interlayers requires an additional circuit element in order to account for the appearance of a third feature at the low-frequency region (Fig. 2a). In previous studies, a Warberg diffusional element was used to model the spectra [10]. However, because this element is mathematically similar to a parallel RC circuit and because it provided an equivalent fit to the data; a circuit diagram containing three parallel RC circuits in series was chosen for simplicity (Fig. 3b) [12].

Examination of Fig. 2 clearly shows significant semicircular features associated with higher double-layer capacitance (C_{dl}) and charge transfer resistance (R_{ct}) for anode and cathode of the specimen lacking electrode/electrolyte interlayers. In these specimens, it is assumed that electro-active area between the junctions of the electrode and electrolyte interfaces are limited and that the charge-transfer reactions at the interfaces become rate-determining; as such diffusional effects are not pronounced. However, when anode/cathode interlayers are incorporated (2a) a significant reduction in C_{dl} and R_{ct} was observed along with the appearance of a third, low-frequency feature. It is thought that when electrode/electrolyte interlayers are added, the intrinsic area of the interfaces is significantly increased, accelerating the charge-transfer reactions at the interfaces. Diffusion phenomenon would then be expected to become important, especially at higher current densities.

3.1. Temperature dependence of five-layer specimens

Characterization experiments were performed on five-layer assemblies in order to provide a greater understanding of how the addition of these interlayer regions improves electrochemical performance. Polarization curves for samples containing thin anode and cathode interlayers were obtained as a function of temperature and the results are presented in Fig. 4. Unlike three-layer assemblies, the samples containing interlayers exhibited "typical" polarization behavior with an initial, non-linear drop associated with activation polarization followed by a linear ohmic region. Reactant flow rates were kept sufficiently high as to eliminate the impact of concentration polarization at high current densities. A non-linear least squares (NLLS) regression approach was applied to these curves in order to attempt to quantify the relative magnitude of relevant electrochemical parameters. The parameters used to fit the data were extracted

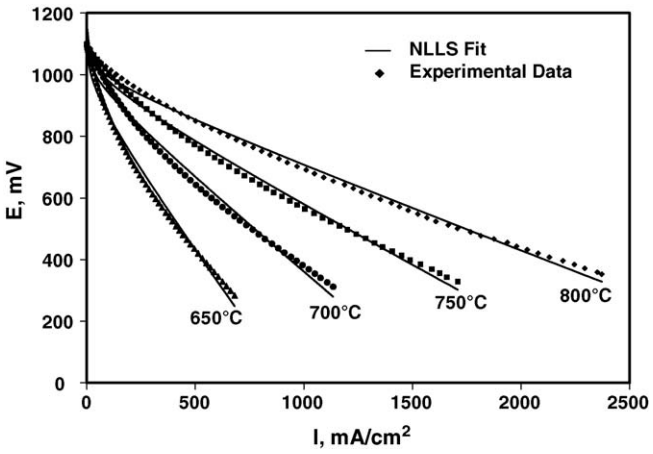

Fig. 4. Polarization curves of single SOFC button cell (five-layer assembly) as a function of temperature.

from the general expression describing the observed potential (E_{obs}) in a two electrode cell:

$$E_{obs} = E_r - \eta_a - \eta_c - \eta_\Omega \quad (1)$$

where E_r is the thermodynamic reversible potential for the cell (i.e., open circuit voltage), η_a is the anodic overpotential, η_c is the cathodic overpotential, η_Ω is ohmic overpotential ($\eta_\Omega = i \cdot R$), and R is the area specific ohmic resistance (ASOR). Since the working surface area of the anode is far larger than that of the cathode for the present button cell configuration (i.e., $i_a \ll i_c$), and, furthermore, oxygen reduction is generally considered more sluggish than hydrogen oxidation, we tentatively assume $\eta_a \ll \eta_c$, thus Eq. (1) becomes,

$$E_{obs} \approx E_r - \eta_c - iR \quad (1')$$

For the thin and porous cathode at high reactant flow rates, the mass-transfer effect is assumed to be negligible, and the cathode overpotential (η_c) is mainly associated with charge-transfer phenomena,

$$\eta_c \approx -\frac{RT}{\alpha n F} \ln i^\circ + \frac{RT}{\alpha n F} \ln i = -b \log i^\circ + b \log i \quad (2)$$

Eq. (2) is a simplified version of the Bulter–Volmer equation. Substitute Eq. (2) into Eq. (1′), we get

$$E_{obs} \approx (E_r + b \log i^\circ) - b \log i - iR \quad (3)$$

$$E_{obs} \approx E_0 - b \log i - iR \quad (3')$$

The parameters b and i_0 are the Tafel slope and exchange current density of the cathode and address only the kinetics of the oxygen reduction reaction. The combined real resistance, (ASOR), is related to the linear decrease in potential as a function of current density and is primarily associated with assembly resistance but is also affected by the resistance of the testing apparatus. This approach has been presented in the literature regarding polymer electrolyte fuel cells (PEMFC) and has been found to provide a good match to experimental polarization data for current densities sufficiently far from the limiting current density for these systems [13–15]. Upon close examination of

Table 1
Electrochemical parameters calculated from non-linear least squares regression of five-layer cell polarization data as a function of temperature

Temperature (°C)	E_0 (mV)	$b_{cathode}$ (mV dec^{-1})	R (Ω cm^2)
650	1124	80.2	0.95
700	1114	60.2	0.58
750	1119	51.8	0.37
800	1118	48.9	0.26

Fig. 4 it is evident that this model provides an inadequate fit to the data primarily because it does not account for contributions associated with the anode. In PEMFCs, the oxidation of hydrogen is nearly reversible over platinum and platinum alloy catalysts. SOFCs based upon nickel metal cerments, however, appear to exhibit greater activation resistance presumably due to the increased rigors of the multi-step reaction pathway, low metal surface area, and removal of steam from active catalytic sites. As such, the Tafel parameters predicted via this modeling approach should be expected to underestimate the Tafel slope and accounts for the failure of the model to successfully follow the nonlinear, low current density portion of the polarization curve. In fact, the Tafel slopes predicted through this modeling approach were lower than the theoretical values of 91.2 mV dec^{-1} at 650 °C and 106 mV dec^{-1} at 800 °C. ASOR values extracted from NLLS analysis were 0.26 and 0.95 Ω cm^2 for the five-layer and three-layer specimens, respectively. Relevant electrochemical parameters obtained via this modeling approach are presented in Table 1.

Upon examination of these data it can be observed that each of these parameters appear to depend upon temperature in a consistent manner. E_0, primarily associated with the reversible potential of hydrogen oxidation reaction, E_r, decreased with increasing temperature which is consistent with that predicted by thermodynamic calculations. The Tafel slope decreased with increasing temperature which is associated with decreased kinetic resistance and decreased adsorbed steam surface coverage. ASOR of the assembly yielded an Arrhenius temperature dependence which is evidenced in Fig. 5. This ohmic contribution accounts for all of the ohmic losses in the fuel cell which include current collection and leads.

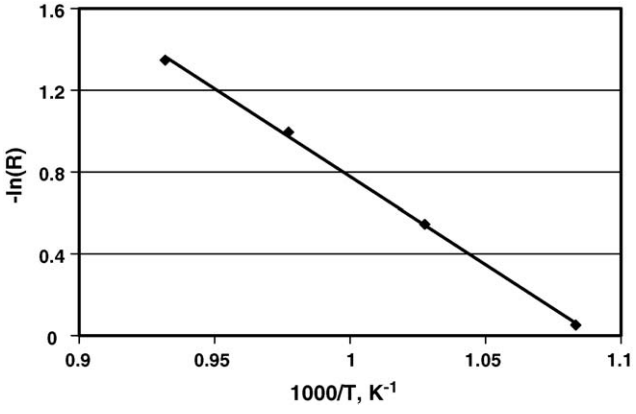

Fig. 5. Arrhenius dependence of area specific ohmic resistance (Ω cm^2) for single SOFC button cell (five-layer assembly).

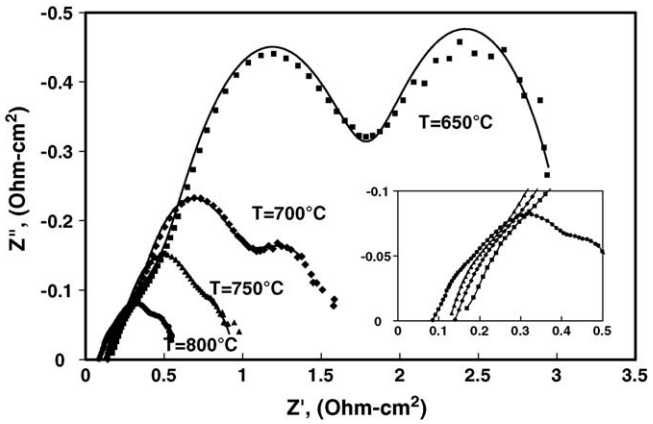

Fig. 6. Impedance spectra obtained for single SOFC button cell (five-layer assembly) as a function of temperature (callout provides additional detail in high frequency region).

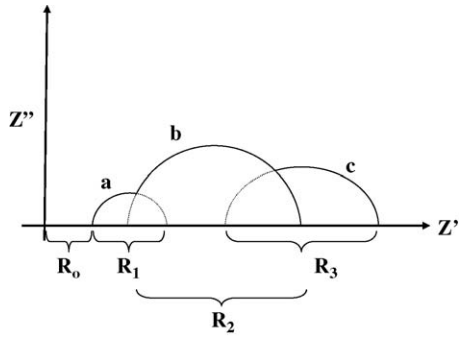

Fig. 7. Resolved impedance spectra illustrating overlapping semicircular features which are not completely isolated by frequency, (a) high-frequency feature, (b) mid-range frequency feature, (c) low-frequency feature.

Impedance spectra were taken as a function of temperature for five-layer specimens and the results are presented in Fig. 6. As mentioned previously, samples which incorporate anode and cathode interlayers clearly show three distinct time constants as evidenced by the three semicircular features. These spectra were modeled using the modified Randal circuit element (Fig. 3b) which provided good correlation with the data but, for brevity, the regressed parameters are not presented in this publication. Most notable is the apparent non-linearity of the 2nd and 3rd semicircular features as a function of temperature showing that temperature has a disproportionate influence upon the 3rd feature compared to the 2nd. Because insertion of a reference electrode was difficult, it was not possible to explicitly assign a particular electrochemical process (diffusion, charge transfer, etc.) to its EIS feature. However, it can be reasoned that diffusion phenomenon exhibits a linear dependence upon temperature while kinetic processes vary exponentially suggesting that the third feature is likely associated with a kinetic process, presumably on the cathode. This determination is consistent with previous determinations through variations of cathode gas compositions. No specific determination could be made on the high frequency or mid-range frequency features; however, previous literature has suggested that they are related to anodic processes [11]. The high frequency intercepts at axis Z', R_0, normally associated with ohmic losses within the cell, were consistent in trend with ASOR values calculated from the polarization curves, but were 53% lower in magnitude. This is probably due to the limitations of the NLLS model given that anode overpotential was neglected.

EIS data was used to deconvolute the relative impedances of component processes in a typical five-layer SOFC assembly as a function of temperature and polarization. It was assumed that for the purposes of this model, each of the EIS spectra consisted of 3 semicircular features which overlapped slightly in the frequency domain (Fig. 7).

Additionally, because it was apparent that additional distributed elements were contained throughout each spectrum, constant phase elements (CPE) were used in place of typical capacitor elements. The regressed parameters obtained when the impedance spectra from temperature and polarization experiments was fit to the modified Randal's circuit was used to estimate the extent of cathodic, anodic, and ohmic resistances. These data are presented in Tables 2 and 3.

Table 2
Contribution of component real impedances for a five-layer SOFC assembly as a function of temperature at OCV

Vs. temp (°C)	% of total resistance or overpotential			
	IR	*a*	*b*	*c*
650	5.5	8.0	48.6	37.9
700	8.6	10.4	39.3	41.7
750	13.6	7.9	53.4	25.1
800	17.2	8.9	43.0	30.9

As discussed previously, ohmic resistance of the five-layer cell exhibited an Arrhenius dependence with temperature. However, the ohmic component did increase as a relative percentage of the total impedance of this cell as a function of temperature from a minimum of 5.5% at 650 °C to a maximum contribution of 17.2% at 800 °C (Table 2). This trend is observed because the kinetic resistances, presumbably contributions of the 1st and 3rd impedance features are significantly more temperature dependant than the ohmic losses. The 3rd semicircular feature, previously associated with cathodic processes, was observed to decrease in percentage of total impedance with temperature. The 1st and 2nd EIS features did not exhibit any clear trend within experimental uncertainty for the temperature experiments.

Table 3
Contribution of component real impedances for a five-layer SOFC assembly as a function of polarization at 800 °C

Vs. OCV (−mV)	% of total resistance or overpotential			
	IR	*a*	*b*	*c*
0	17.2	8.9	43.0	30.9
100	21.6	8.6	46.1	23.7
200	24.6	7.6	49.5	18.2
300	25.8	8.5	49.0	16.8
400	25.2	12.9	45.4	16.6

Table 4
Example impedance parameters calculated from model fitting for five-layer SOFCs as a function of polarization at 800 °C

Bias vs. OCV	R_0 (Ω cm^2)	R_1 (Ω cm^2)	C_1 (F cm^{-2})	α_1	R_2 (Ω cm^2)	C_2 (F cm^{-2})	α_2	R_3 (Ω cm^2)	C_3 (F cm^{-2})	α_3
0	0.10	0.052	0.0017	0.80	0.25	0.031	0.62	0.18	0.72	0.58
0.1	0.10	0.040	0.0002	0.95	0.21	0.024	0.64	0.11	0.86	0.61
0.2	0.10	0.031	0.0004	0.94	0.20	0.033	0.59	0.07	1.09	0.67
0.3	0.10	0.033	0.0005	0.92	0.19	0.040	0.57	0.07	1.29	0.70
0.4	0.11	0.051	0.0006	0.87	0.08	0.007	0.83	0.14	0.86	0.47

3.2. Polarization effects of five-layer specimens

The effect of polarization was examined for typical five-layer assemblies at 800 °C and the results are shown in Fig. 8. Good correlation of the data to the extended Randal circuit element was observed (Fig. 3b). The impedance parameters calculated using the described circuit models are presented in Table 4. The imaginary impedance components (1/ωC) of the second and third features appear to decrease proportionately with polarization which is in stark contrast to their relative variation as a function of temperature described previously. As discussed in the previous sections, the third feature was attributed to a cathodic process through experimentation and review of literature [11].

Similar to the temperature experiments, EIS was used to deconvolute the relative impedances of the component processes. In each calculation, the individual real resistance term (R_0, R_1, R_2 or R_3) was determined via EIS and their relative contributions were calculated as a function of current density. The results of these models are plotted as a function of current density in Fig. 9. Cathodic overpotentials (c) averaged 21.2% over the range of polarization. The cathodic contribution exhibited a decreasing trend with polarization which is consistent with the notion that the EIS semicircular 3rd feature is associated with electro-catalytic processes. The ohmic contribution was determined to be approximately 23% over the range of polarization values. While the magnitude of ohmic resistance was constant as a function of current density, its relative contribution increased illustrating the effect of high current densities on electrolyte conduction. The high frequency feature contributed approximately 9% of the total impendence as a function of polarization with no observable trend. It is assumed that this feature is associated with anodic reactions from previous experimentation, though this conclusion cannot be substantiated via this approach. The mid-range frequency feature represents the most significant contribution accounting for nearly 47% of the total impedance. The magnitude of the impedance increased linearly with current density suggesting that this feature is associated with charge transfer processes which could be either cathodic or anodic.

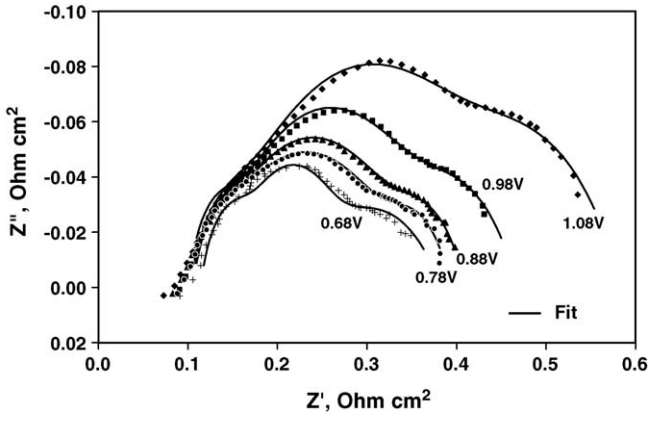

Fig. 8. Impedance spectra obtained for single SOFC button cell (five-layer assembly) as a function of polarization at 800 °C.

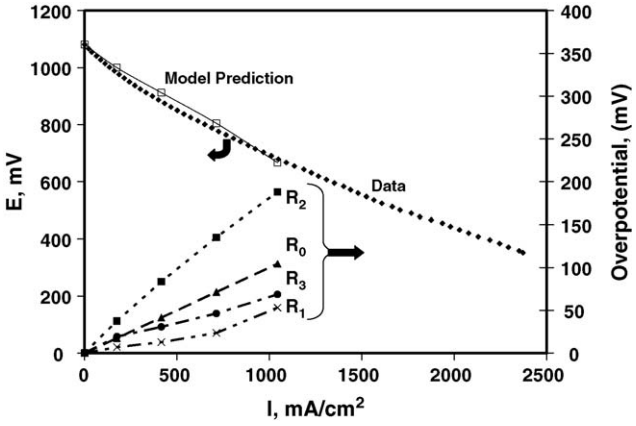

Fig. 9. Polarization curve for single SOFC button cell (five-layer assembly) incorporating impedance model and specific contributions of individual spectral components at 800 °C (R_1), high-frequency contribution (R_2), mid-range frequency contribution, (R_3) low-frequency contribution, (R_0) ohmic contribution.

4. Conclusions

The inclusion of interfacial electrode layers on the fuel cell electrodes significantly improved the performance of anode supported cells. Specimens without an interlayer (three-layer-cell) exhibited far greater impedances than the five-layer specimen. The OCV was lower for the three-layer specimen attesting to increased difficulty generating a hermetic seal in these specimens for equivalent electrolyte thicknesses. Impedance spectra illustrated that the cathode for the three-layer specimen exhibited considerable double-layer capacitance and charge transfer resistance which was very small for the five-layer specimen with electrode/electrolyte interlayers. Incorporating the interfacial layers decreases these impedances largely by introduction of the diffuse mixed conduction region at the electrode/electrolyte interface. Because the bulk cathode material, LSM is predominately an electron conductor, this behavior is especially apparent at the cathode.

Five-layer assemblies were evaluated as a function of temperature and polarization to increase understanding of the

role of the electrode/electrolyte interlayer. Ohmic resistances decreased with temperature consistent with that predicted from the Arrhenius law but exhibited no trend with polarization. Values of ohmic polarization were observed to be close to R_0 obtained from EIS. EIS showed evidence of three distinct features which were attributed to different time-dependant processes within the fuel cell. Temperature appeared to impact each of these features to differing extents with a far greater dependence associated with the 3rd EIS semicircular feature relative to the high and mid-range frequency features. This observation is associated with a significant change in the double-layer capacitance which was attributed to the cathode interface. Polarization experiments showed only modest variations in the features' relative impedances with increasing current density. These data appear to suggest that the 1st and 3rd semicircular features are associated with kinetic processes while the real component of the 2nd feature is attributed to charge transfer resistance.

EIS data was used to deconvolute the relative contribution of these impedances. For thin film five-layer assemblies, charge transfer resistance (2nd feature) appear to contribute most significantly to the overall impedance at OCV. Cathodic kinetic resistances also contributes significantly to the observed resistance, however, its relative significance decreases rapidly once the cell is polarized due to the enhanced driving force for reaction. Ohmic contributions are still rather considerable for these assemblies even though an electrolyte thickness of $<10\ \mu m$ was achieved. Contrary to results obtained for low temperature PEMFCs, anode contributions cannot be neglected under the conditions of this study. EIS data suggest that as much as 12% of the total impedance can be associated with anode kinetics. As such, models which neglect these activation losses will tend to under-estimate Tafel coefficients providing unacceptable fits in the Tafel region.

References

[1] S. Colson-Inam, Fuel Cell Today 1 (1) (2004).
[2] J. Larminie, A. Dicks, Fuel Cell Systems Explained, John Wiley and Sons Ltd., West Sussex, 2003.
[3] J.W. Kim, A.V. Virkar, K.Z. Fung, K. Mehta, S.C. Singhal, J. Electrochem. Soc. 146 (1999) 69–78.
[4] S. De Souza, S.J. Visco, J.C. DeJonghe, J. Electrochem. Soc. 144 (2001) A788–A794.
[5] Y.J. Leng, S.H. Chan, K.A. Khor, S.P. Jiang, Int. J. Hydrogen Energy 29 (2004) 1025–1033.
[6] S. Adler, Chem. Rev. 104 (2004) 4791–4843.
[7] D. Schmidt et al., US Patent 6,984,467.
[8] F. Zhao, A. Virkar, J. Power Sources 141 (2005) 79–95.
[9] J.D. Kim, G.D. Kim, J.W. Moon, Y.I. Park, W.H. Lee, K. Kobayashi, M. Nagai, C.E. Kim, Solid State Ionics 143 (2001) 379–389.
[10] H. Xiao, T.L. Reitz, In Solid-State Ionic Devices I.V., in: E.D. Wachsman, F.H. Garzon, E. Traversa, R. Mukundan, V. Birss (Eds.), The Electrochemical Society Proceedings Series, NJ, 2005.
[11] N. Wagner, W. Schnurnberger, B. Muller, M. Lang, Electrochim. Acta 43 (24) (1998) 3785–3793.
[12] A.J. Bard, L.R. Faulkner, Electrochemical Methods, in: Fundamentals and Applications, Wiley, New York, 1980.
[13] S. Srinivasan, E.A. Ticianelli, C.R. Derouin, A. Redondo, J. Power Sources 22 (1988) 359.
[14] J. Kim, S.M. Lee, S. Srinivasan, C. Chamberlin, J. Electrochem. Soc. 142 (8) (1995).
[15] P. Costamagna, C. Yang, A. Bocarsly, S. Srinivasan, Electrochim. Acta 47 (2002).